



Self-calibrated evaporation-based disaggregation of SMOS soil moisture: An evaluation study at 3 km and 100 m resolution in Catalunya, Spain

Olivier Merlin, Maria-José Escorihuela, Miquel Aran Mayoral, Olivier Hagolle, Al Bitar Ahmad, Yann H. Kerr

► To cite this version:

Olivier Merlin, Maria-José Escorihuela, Miquel Aran Mayoral, Olivier Hagolle, Al Bitar Ahmad, et al.. Self-calibrated evaporation-based disaggregation of SMOS soil moisture: An evaluation study at 3 km and 100 m resolution in Catalunya, Spain. Remote Sensing of Environment, 2012, pp.10.1016/j.rse.2012.11.008. 10.1016/j.rse.2012.11.008 . hal-00759849

HAL Id: hal-00759849

<https://hal.science/hal-00759849v1>

Submitted on 3 Dec 2012

HAL is a multi-disciplinary open access archive for the deposit and dissemination of scientific research documents, whether they are published or not. The documents may come from teaching and research institutions in France or abroad, or from public or private research centers.

L'archive ouverte pluridisciplinaire **HAL**, est destinée au dépôt et à la diffusion de documents scientifiques de niveau recherche, publiés ou non, émanant des établissements d'enseignement et de recherche français ou étrangers, des laboratoires publics ou privés.

Self-calibrated evaporation-based disaggregation of SMOS soil moisture: an evaluation study at 3 km and 100 m resolution in Catalunya, Spain

Olivier Merlin, Maria José Escorihuela, Miquel Aran Mayoral, Olivier Hagolle, Ahmad Al Bitar, and Yann Kerr

O. Merlin is with the Centre d'Etudes Spatiales de la Biosphère (CESBIO), Toulouse, France; email: olivier.merlin@cesbio.cnes.fr

Abstract

A disaggregation algorithm is applied to 40 km resolution SMOS (Soil Moisture and Ocean Salinity) surface soil moisture using 1 km resolution MODIS (MODerate resolution Imaging Spectroradiometer), 90 m resolution ASTER (Advanced Spaceborne Thermal Emission and Reflection radiometer), and 60 m resolution Landsat-7 data. DISPATCH (DISaggregation based on Physical And Theoretical scale CHange) distributes high-resolution soil moisture around the low-resolution observed mean value using the instantaneous spatial link between optical-derived soil evaporative efficiency (ratio of actual to potential evaporation) and near-surface soil moisture. The objective is three-fold: (i) evaluating DISPATCH at a range of spatial resolutions using readily available multi-sensor thermal data, (ii) deriving a robust calibration procedure solely based on remotely sensed data, and (iii) testing the linear or nonlinear behaviour of soil evaporative efficiency. Disaggregated soil moisture is compared with the 0-5 cm in situ measurements collected each month from April to October 2011 in a 20 km square spanning an irrigated and dry

land area in Catalunya, Spain. The target downscaling resolution is set to 3 km using MODIS data and to 100 m using ASTER and Landsat data. When comparing 40 km SMOS, 3 km disaggregated and 100 m disaggregated data with the in situ measurements aggregated at corresponding resolution, results indicate that DISPATCH improves the spatio-temporal correlation with in situ measurements at both 3 km and 100 m resolutions. A yearly calibration of DISPATCH is more efficient than a daily calibration. Assuming a linear soil evaporative efficiency model is adequate at kilometeric resolution. At 100 m resolution, the very high spatial variability in the irrigated area makes the linear approximation poorer. By accounting for non-linearity effects, the slope of the linear regression between disaggregated and in situ measurements is increased from 0.2 to 0.5. Such a multi-sensor remote sensing approach has potential for operational multi-resolution monitoring of surface soil moisture and is likely to help parameterize soil evaporation at integrated spatial scales.

Keywords: disaggregation, downscaling, SMOS, MODIS, ASTER, Landsat, evaporation, calibration, irrigation

1. Introduction

The current climatic trend and variability bring a questioning look to the natural supply of water resources. The point is that monitoring water resources requires observation strategies at a range of spatial scales: the atmospheric (global circulation model grid) scale, the hydrologic (catchment) scale, the administrative (irrigation area) scale and the local (field) scale. The only feasible way to provide multi-scale data sets over extended areas is through multi-sensor/multi-resolution remote sensing.

9 Among the variables accessible from remote sensing, soil moisture is cru-
10 cial in hydrology as it controls evaporation, infiltration and runoff processes
11 at the soil surface. However, the operational retrieval of soil moisture is
12 currently made from passive microwave sensors at a resolution of several
13 tens of km only. In particular, the surface soil moisture retrieved from
14 C-band AMSR-E (Advanced Microwave Scanning Radiometer-EOS, Njoku
15 et al. (2003)) data and L-band SMOS (Soil Moisture and Ocean Salinity,
16 Kerr et al. (2012)) data has a spatial resolution of about 60 km and 40 km,
17 respectively. The forthcoming SMAP (Soil Moisture Active and Passive, En-
18 tekhabi et al. (2010)) mission, scheduled for launch in 2014, will provide soil
19 moisture data at 10 km resolution.

20 Optical sensors offer a wide range of spatial resolutions from several tens
21 of meters for Landsat and ASTER (Advanced Spaceborne Thermal Emission
22 and Reflection radiometer) to 1 km for MODIS (MODerate resolution Imag-
23 ing Spectroradiometer). Although optical data have potential to monitor soil
24 moisture, their sensitivity to other environmental factors (especially meteo-
25 rological conditions and vegetation cover) makes the soil moisture retrieval
26 impractical. Nevertheless, the synergy between low-resolution microwave
27 and high-resolution optical data (Zhan et al., 2002) is likely to help achieve
28 a multi-resolution soil moisture retrieval approach.

29 Microwave/optical data merging methods for estimating high-resolution
30 soil moisture are generally based on the triangle (Carlson et al., 1994) or
31 trapezoid (Moran et al., 1994) approach. Both similarly relate the varia-
32 tions in land surface temperature to the variations in soil water content and
33 vegetation cover (Carlson, 2007; Petropoulos et al., 2009). In the trapezoid

34 approach however, the fraction of water-stressed vegetation is added as a
35 third variable to explain a possible increase of vegetation temperature above
36 the temperature of fully vegetated well-watered pixels.

37 By gathering triangle- and trapezoid-based method groups, two types of
38 microwave/optical data merging approaches can be distinguished according
39 to their purely-empirical (polynomial-fitting, Chauhan et al. (2003)) or semi-
40 physical (evaporation-based, Merlin et al. (2008)) nature. The polynomial-
41 fitting approach consists in i) expressing high-resolution soil moisture as a
42 polynomial function of optical-derived variables (land surface temperature,
43 vegetation index, surface albedo) available at high resolution, ii) applying
44 the polynomial expression at low resolution to determine fitting parameters
45 and iii) applying the polynomial at high resolution using low-resolution fitted
46 parameters. Note that the polynomial-fitting approach is rather a synergis-
47 tic approach combining microwave and optical data than a disaggregation
48 method because the conservation law is in general not satisfied at low resolu-
49 tion: due to the nonlinear nature of the polynomial function, the average of
50 the estimated high-resolution soil moisture is not equal to the low-resolution
51 observation. The evaporation-based approach uses the same optical-derived
52 variables as the polynomial-fitting approach. However, it makes an attempt
53 to physically represent the spatial link between optical-derived evaporation
54 efficiency (ratio of actual to potential evaporation) and surface soil mois-
55 ture. Note that other ancillary (soil and meteorological) data may be used
56 in addition to optical data to help represent the spatio-temporal relation-
57 ship between optical-derived evaporation efficiency and surface soil moisture
58 (Merlin et al., 2008).

59 Piles et al. (2011) recently developed a new polynomial-fitting method by
 60 merging SMOS and MODIS data to provide surface soil moisture data at 10
 61 km and 1 km resolution. The approach was based on Chauhan et al. (2003)
 62 except that high-resolution optical-derived surface albedo was replaced by
 63 low-resolution microwave brightness temperature in their polynomial func-
 64 tion. The method in Piles et al. (2011) was applied to the AACES (Australian
 65 Airborne Cal/Val Experiments for SMOS, Peischl et al. (2012)) area during
 66 the SMOS commissioning phase. The polynomial coefficients were first de-
 67 termined at low resolution by applying the polynom to SMOS-scale bright-
 68 ness temperature, the MODIS land surface temperature aggregated at SMOS
 69 resolution and the MODIS-derived fraction vegetation cover aggregated at
 70 SMOS resolution. This step required to correct SMOS soil moisture prod-
 71 uct using in situ soil moisture measurements, in order to remove any bias in
 72 SMOS data. The polynomial expression was then applied at high-resolution
 73 to SMOS brightness temperature and optical data. This step required to
 74 over-sample 40 km resolution SMOS brightness temperature at 1 km reso-
 75 lution. Piles et al. (2011) indicated that i) introducing the low-resolution
 76 SMOS brightness temperature into the polynomial function reduced the bias
 77 between downscaled and in situ soil moisture and ii) the spatio-temporal
 78 correlation between SMOS and in situ measurements was slightly degraded
 79 when applying the polynomial-fitting method.

80 Kim and Hogue (2012) recently developed a new evaporation-based disag-
 81 gregation (named UCLA) method of microwave soil moisture product. The
 82 approach was based on the formulation of evaporative fraction derived by
 83 Jiang and Islam (2003), and a linear scaling relationship between evapora-

84 tive fraction and surface soil moisture. The originality of the UCLA method
85 relied in the representation of vegetation water stress at low resolution to de-
86 rive a high-resolution soil wetness index (trapezoid approach), whilst previous
87 evaporation-based methods assumed an unstressed vegetation cover (trian-
88 gle approach). The algorithm was applied to AMSR-E level-3 soil moisture
89 product (Njoku et al., 2003) using 1 km resolution MODIS data over the ~ 75
90 km by 50 km SMEX04 area (Jackson et al., 2008), and the 1 km resolution
91 disaggregated data were evaluated at the 36 SMEX sampling sites. In their
92 paper, the authors compared the UCLA method to a range of polynomial-
93 fitting algorithms (Chauhan et al., 2003; Hemakumara et al., 2004; Hossain
94 and Easson, Jul. 2008) and to the evaporation-based method in Merlin et al.
95 (2008). Results indicated that i) both evaporation-based methods (Kim and
96 Hogue, 2012; Merlin et al., 2008) significantly improved the limited spa-
97 tial variability of AMSR-E product and ii) the polynomial-fitting algorithms
98 showed poorer performance over the SMEX04 area.

99 Merlin et al. (2012b) recently improved the evaporation-based method de-
100 veloped in Merlin et al. (2008). DISPATCH (DISaggregation based on Physi-
101 cal And Theoretical scale CHange) estimated high-resolution soil evaporative
102 efficiency using high-resolution land surface temperature and NDVI data and
103 the low-resolution temperature endmembers derived from high-resolution op-
104 tical data. The link between optical data and surface soil moisture was then
105 ensured by a nonlinear soil evaporative efficiency model, which was calibrated
106 using available remote sensing data only. The four main improvements made
107 in Merlin et al. (2012b) consisted in integrating a representation of: vegeta-
108 tion water stress at high resolution using the methodology in Moran et al.

109 (1994), the low-resolution sensor weighting function, the oversampling of
110 low-resolution microwave data, and the uncertainty in output disaggregated
111 data. DISPATCH was applied to version-4 SMOS level-2 soil moisture over
112 the AACES area using 1 km resolution optical MODIS data, and the 1 km
113 resolution disaggregated data were evaluated on a daily basis against 1 km
114 resolution aggregated in situ measurements during the one-month summer
115 and winter AACES. Results indicated a mean spatial correlation coefficient
116 between 1 km resolution disaggregated SMOS and in situ data of about 0
117 during the winter AACES and 0.7-0.8 during the summer AACES.

118 The development of optical-based disaggregation approaches of microwave-
119 derived soil moisture is still at its beginnings and more evaluation studies are
120 needed. In particular, the ground data sets used to validate disaggregation
121 methods (Chauhan et al., 2003; Piles et al., 2011; Kim and Hogue, 2012;
122 Merlin et al., 2012b) have been limited to a one-month period although the
123 performance of optical-based methodologies mostly relies on the atmospheric
124 evaporative demand, which greatly varies across seasons. Also, most recent
125 optical-based approaches have been tested using MODIS data although hy-
126 drologic and agricultural applications may require soil moisture data at a spa-
127 tial resolution finer than 1 km. Last, few studies (Merlin et al., 2010c; Piles
128 et al., 2011; Merlin et al., 2012b) have applied disaggregation approaches to
129 SMOS soil moisture products whereas downscaling strategies may contribute
130 to the SMOS calibration/validation by reducing the large mismatch in spa-
131 tial extent between 40 km resolution SMOS observations and localized in situ
132 measurements.

133 In this context, this paper seeks to (i) evaluate DISPATCH at a range

134 of spatial resolutions using readily available multi-sensor thermal data, (ii)
 135 derive a robust calibration procedure solely based on remotely sensed data,
 136 and (iii) test the linear or nonlinear behaviour of soil evaporative efficiency.
 137 DISPATCH is applied to last released version-5 SMOS level-2 soil moisture
 138 product over an irrigated and dry land area in Catalunya, Spain. The ob-
 139 jective is to provide 1 km resolution surface soil moisture over a 60 km by
 140 60 km area from 40 km resolution SMOS and 1 km resolution MODIS data
 141 and to provide 100 m resolution surface soil moisture over a 20 km by 20
 142 km area from MODIS-disaggregated SMOS and 100 m resolution re-sampled
 143 ASTER and Landsat-7 data. Disaggregated soil moisture data are evaluated
 144 at 3 km resolution using in situ 0-5 cm measurements made once a month
 145 from April to October 2011, and at 100 m resolution using the ground data
 146 collected in August, September and October. In this study, ASTER data are
 147 considered as reference high-resolution data to evaluate the performance of
 148 DISPATCH when applied to high-quality land surface temperature data and
 149 to more operational Landsat thermal data.

150 The paper is organized as follows. Data sets are first described (section
 151 2). Next, four different modes of DISPATCH are presented: the LINEAR
 152 and NONLINEAR modes (for linear or nonlinear soil evaporative efficiency
 153 model) and the DAILY and YEARLY modes (for daily or yearly calibration
 154 procedure) (section 3). Then, the linearity of soil evaporative efficiency model
 155 and its calibration procedure are tested at 3 km and 100 m resolution (section
 156 4). Finally, an insight is given about the parameterization of soil evaporative
 157 efficiency from microwave/thermal combined remote sensing data (section
 158 5). Last, the conclusions and perspectives are presented (section 6).

159 2. Data

160 The 60 km by 60 km study area is located east of Lleida in Catalunya,
161 Spain. Lleida has arid continental Mediterranean climate typical of the Ebro
162 Valley, with a mean yearly air temperature of 16°C, precipitation of 400 mm,
163 and number of days with rain of 60. Field experiments were undertaken
164 over a focus 20 km square area, centered on the broader 60 km study area.
165 The 20 km square area was chosen so that it includes irrigated crops, it is
166 relatively flat and far enough (more than 100 km) from the Pyrenees and
167 the Mediterranean sea to limit topographic and coastal artifacts in SMOS
168 data. It spans part of the 700 km² Urgell irrigation area and the surrounding
169 dryland area, which both represent about half of the 20 km square. Irrigated
170 crops include wheat, maize, alfalfa and fruit (apple and pear) trees while
171 dryland crops are mainly barley, olive trees, vineyards and almond trees. An
172 overview of the study area is presented in Figure 1.

173 2.1. *In situ*

174 The 0-5 cm soil moisture was measured using the gravimetric technique
175 during seven one- (or two-) day campaigns in 2011: on DoY (Day of Year)
176 97-98, DoY 146-147, DoY 164-165, DoY 196, DoY 228-229, DoY 244, and
177 DoY 277. Each field campaign was undertaken on the same sampling grid
178 (see Figures 1c and 1d), which represented 120 soil moisture measurement
179 (sampling) points within the 20 km square. The total sampling extent cov-
180 ered four 3 km by 3 km areas, with two located in the irrigated area and the
181 other two in the dryland area. Each 3 km square was sampled by ten sam-
182 pling points approximately spaced by 1 km, and three separate soil moisture

183 measurements were made at each sampling point. Soil texture was derived
184 from particle size analysis at each of the 120 sampling points with a mean
185 clay and sand fraction of 0.24 and 0.37, respectively. The approach in Sax-
186 ton et al. (1986) was used to convert gravimetric measurements to volumetric
187 values with a mean soil density estimated as 1.37 g cm^{-3} . Table 1 reports
188 the spatial and temporal variations of 0-5 cm soil moisture obtained during
189 the 2011 campaign in the dryland and irrigated area separately.

190 *2.2. Remote sensing*

191 The version-5.01 SMOS level-2 soil moisture product released on March
192 16, 2012 is used. Details on the processing algorithms can be found in the
193 Algorithm Theoretical Baseline Document (ATBD, version 3.4, Kerr et al.
194 (2011)), and on the L2SM products structure in the SMOS Level 2 and Aux-
195 iliary Data Products Specifications (SO-TN-IDR-GS-0006, Issue 6.0 2011-05-
196 18). SMOS level-2 soil moisture data are extracted over a 100 km by 100 km
197 area centered on the 20 km square area. Following the SMOS re-sampling
198 strategy described in Merlin et al. (2010c), re-sampled SMOS data overlap
199 four times over the 60 km by 60 km study area.

200 MODIS products MOD11A1, MYD11A1 and MOD13A2 were downloaded
201 through the NASA Warehouse Inventory Search Tool, projected in UTM 31
202 North with a sampling interval of 1000 m using the MODIS reprojection tool
203 and extracted over a 100 km by 100 km area centered on the study area, con-
204 sistent with large scale SMOS data. Figure 2 presents the 1 km resolution
205 images over the study area of Terra NDVI on DoY 225, Terra land surface
206 temperature on DoY 228 (10:30 am) and Aqua land surface temperature on
207 DoY 228 (1:30 pm). Some of the observed variabilities in MODIS tempera-

208 ture data can be attributed to vegetation cover and topographic effects.

209 ASTER overpassed the study area on DoY 228, DoY 244 and DoY 276 at
210 10:30 am local solar time. ASTER official AST_2B3 and AST_2B5 products
211 were downloaded from ASTER Ground Data Segment Information Manage-
212 ment System web site. ASTER 15 m resolution red (band 2) and near-
213 infrared (band 3) bands, and ASTER 90 m resolution radiometric tempera-
214 ture are extracted over the 20 km square and re-sampled at 100 m resolution.
215 NDVI is computed at 100 m resolution as the difference between near-infrared
216 and red re-sampled bands divided by their sum. Since no cloud mask is ap-
217 plied to AST_2B3 and AST_2B5 products, the partially cloudy scene acquired
218 on DoY 244 is discarded. The ASTER scenes acquired on DoY 228 and DoY
219 276 are cloud free. Although ASTER currently provides the best quality land
220 surface temperature data from space, it does not acquire data continuously
221 and data collection is scheduled upon request. Herein, ASTER data are thus
222 considered as reference high-resolution data to evaluate the performance of
223 DISPATCH when applied to (i) high-quality land surface temperature data
224 and (ii) more operational Landsat data.

225 Landsat-7 overpassed the study area on the same dates as ASTER at
226 around 10:30 am local solar time. Landsat level-1 radiances products were
227 downloaded free of charge from USGS Earth Explorer website. They are
228 available at 30 m resolution in all spectral bands. Note that the native res-
229 olution of thermal infrared bands (61 for low gain and 62 for high gain)
230 is 60 m. In this study, Landsat level-1 visible and near-infrared bands are
231 corrected for atmospheric effects with the algorithm in Hagolle et al. (2010),
232 whereas thermal infrared level-1 radiances are processed without atmospheric

233 correction. The rationale for neglecting atmospheric effects in thermal data
 234 is based on Merlin et al. (2012b), who used the MODIS radiance-derived
 235 brightness temperature at sensor level instead of MODIS level-2 land surface
 236 temperature as input to DISPATCH. Their results indicated that correcting
 237 land surface temperature data for atmospheric effects is not a necessary step
 238 as long as the disaggregation is based on temperature differences within a
 239 40 km size area (SMOS pixel). Herein, Landsat radiance-derived land sur-
 240 face temperature T is hence estimated from band 62 (high gain) by simply
 241 computing the inverse Planck function:

$$T = \frac{K_2}{\ln(\frac{K_1}{R_\lambda} + 1)} \quad (1)$$

242 with $K_1 = 666.09 \text{ W m}^{-2} \text{ sr}^{-1} \mu\text{m}^{-1}$ and $K_2 = 1282.71 \text{ K}$ for band 62, and
 243 R_λ the spectral radiance in $\text{W m}^{-2} \text{ sr}^{-1} \mu\text{m}^{-1}$ converted from digital number
 244 (DN):

$$R_\lambda = R_{min} + (R_{max} - R_{min}) \times \frac{DN - 1}{255 - 1} \quad (2)$$

245 with $R_{min} = 3.20 \text{ W m}^{-2} \text{ sr}^{-1} \mu\text{m}^{-1}$ and $R_{max} = 12.65 \text{ W m}^{-2} \text{ sr}^{-1} \mu\text{m}^{-1}$
 246 for band 62. Landsat-7 30 m resolution red (band 3), 30 m resolution near-
 247 infrared (band 4), and the 30 m resolution land surface temperature derived
 248 from Equation (1) are extracted over the 20 km square area and re-sampled
 249 at 100 m resolution. NDVI is computed at 100 m resolution as the difference
 250 between near-infrared and red re-sampled bands divided by their sum. The
 251 spatial extent of Landsat-7 data within the 20 km square area is delimited by
 252 the field of view, the contour of clouds detected by the algorithm in Hagolle
 253 et al. (2010) on the image acquired on DoY 244 and the data gaps (stripes)

254 due to Scan Line Corrector (SLC) anomaly. Since the SLC anomaly produces
 255 larger data gaps at the edge of the field of view, the processed Landsat-
 256 7 scenes are truncated at 30 km from the 183 km swath center. Figure 3
 257 presents the 100 m resolution images over the 20 km square area of Landsat-
 258 derived NDVI and land surface temperature on DoY 228. Stripes are visible
 259 in the temperature image, but not in the NDVI image because the algorithm
 260 in Hagolle et al. (2010) interpolates shortwave data within the 60 km wide
 261 truncated Landsat-7 field of view. Note that the minimum and maximum
 262 land surface temperatures are significantly different for Landsat and ASTER
 263 data. The difference in temperature range is due mainly to atmospheric
 264 absorption (not taken into account in the derivation of Landsat temperature)
 265 and partly to the slight difference in overpass time (ASTER overpassed the
 266 study area several minutes after Landsat-7). The data coverage fraction
 267 within the 20 km square area is 82%, 57%, 94% on DoY 228, 244, 276,
 268 respectively.

269 **3. DISPATCH**

270 DISPATCH is an improved version of the algorithms in Merlin et al.
 271 (2008), Merlin et al. (2009), Merlin et al. (2010a) and Merlin et al. (2012b).
 272 A detailed description of DISPATCH is provided in Merlin et al. (2012b) so
 273 only the pertinent details are given here.

274 *3.1. Linearity of soil evaporative efficiency model*

275 One major objective of this paper is to test the linear or nonlinear be-
 276 haviour of the soil evaporative efficiency model used the downscaling rela-
 277 tionship:

$$SM = \mathbf{SM} + \left(\frac{\partial SM_{mod}}{\partial SEE} \right)_{SEE=\mathbf{SEE}} \times (SEE - \mathbf{SEE}) \quad (3)$$

278 with SM being the surface soil moisture disaggregated at high resolution,
 279 \mathbf{SM} the low-resolution soil moisture (for clarity, the variables at coarse scale
 280 are written in bold), SEE the optical-derived soil evaporative efficiency (ratio
 281 of actual to potential evaporation), \mathbf{SEE} its average within a low-resolution
 282 pixel and $\partial SM_{mod}/\partial SEE$ the partial derivative of soil moisture with re-
 283 spect to soil evaporative efficiency. In LINEAR mode the partial derivative
 284 in Equation (3) is computed using the simple and linear soil evaporative
 285 efficiency model in Budyko (1956) and Manabe (1969):

$$SEE_{mod} = SM/\mathbf{SM_p} \quad (4)$$

286 with $\mathbf{SM_p}$ being a soil parameter (in soil moisture unit). By inverting Equa-
 287 tion (4), one obtains:

$$SM_{mod} = SEE \times \mathbf{SM_p} \quad (5)$$

288 Note that nonlinear soil evaporative efficiency models (Noilhan and Planton,
 289 1989; Lee and Pielke, 1992; Komatsu, 2003) were used in the previous versions
 290 of DISPATCH (Merlin et al., 2008, 2010a, 2012b). The rationale for choosing
 291 a linear one is two-fold: (i) the model in Equation (4) may be more robust
 292 than a nonlinear model with an erroneous behaviour and (ii) it may help
 293 describe the real behaviour of soil evaporative efficiency via the calibration of
 294 $\mathbf{SM_p}$. To investigate nonlinearity effects, a NONLINEAR mode is proposed
 295 with the following soil evaporative efficiency model:

$$SEE_{mod,nl} = (SM/\mathbf{SM}_{sat})^{\mathbf{P}} \quad (6)$$

296 with \mathbf{P} an empirical parameter and \mathbf{SM}_{sat} the soil moisture at saturation.
 297 The above expression is chosen for its simplicity (it is controlled by 1 em-
 298 pirical parameter only), and its ability to approximately fit the exponential
 299 model in Komatsu (2003), which was successfully implemented in previous
 300 versions of DISPATCH (Merlin et al., 2008, 2010a). In addition, the model
 301 in Equation (6) equals the linear model in Equation (4) for $\mathbf{P} = 1$ and
 302 $\mathbf{SM}_{sat} = \mathbf{SM}_p$. In Equation (6), the soil moisture at saturation is estimated
 303 as in Cosby et al. (1984):

$$\mathbf{SM}_{sat} = 0.489 - 0.126f_{sand} \quad (7)$$

304 with f_{sand} (-) being the sand fraction (set to 0.37). By inverting Equation
 305 (6), one obtains:

$$SM_{mod,nl} = SEE^{1/\mathbf{P}} \times \mathbf{SM}_{sat} \quad (8)$$

306 In NONLINEAR mode, the disaggregated soil moisture SM_{corr} is written as:

$$SM_{corr} = SM - \Delta SM_{nl} \quad (9)$$

307 with SM being the soil moisture disaggregated using the linear model in
 308 Equation (4) and ΔSM_{nl} a correction term:

$$\Delta SM_{nl} = SM_{mod} - SM_{mod,nl} \quad (10)$$

309 By replacing linear and nonlinear models by their expression in Equation (4)
 310 and (6) respectively, one obtains:

$$\Delta SM_{nl} = SEE \times \mathbf{SM}_p - SEE^{1/P} \times \mathbf{SM}_{sat} \quad (11)$$

311 with \mathbf{SM}_p and P being considered as fitting parameters self-estimated by
 312 DISPATCH from multi-sensor remote sensing observations.

313 In LINEAR mode, the soil moisture parameter \mathbf{SM}_p used in Equation
 314 (4) is estimated as \mathbf{SM}/\mathbf{SEE} . In NONLINEAR mode, the exponent param-
 315 eter P used in Equation (6) is estimated as $\ln(\mathbf{SEE})/\ln(\mathbf{SM}/\mathbf{SM}_{sat})$. By
 316 injecting calibrated \mathbf{SM}_p and P in Equation (11), one finally obtains:

$$\Delta SM_{nl} = \frac{SEE}{\mathbf{SEE}} \times \mathbf{SM} - SEE^{\frac{\ln(\mathbf{SM}/\mathbf{SM}_{sat})}{\ln(\mathbf{SEE})}} \times \mathbf{SM}_{sat} \quad (12)$$

317 Figure 4 illustrates differences between the linear and the nonlinear soil
 318 evaporative efficiency model for given values of \mathbf{SM}_p , \mathbf{SM}_{sat} , \mathbf{SM} and \mathbf{SEE} .
 319 For each fine-scale value of SEE within the low resolution pixel, the difference
 320 between inverse soil evaporative efficiency models provide an estimate of
 321 nonlinearity effects (ΔSM_{nl} in Figure 4) on disaggregated soil moisture. Note
 322 that the nonlinear behaviour of soil evaporative efficiency is a fundamental
 323 limitation of the relationship between soil moisture and its disaggregating
 324 parameters in the higher range of soil moisture values.

325 3.2. Calibration procedure

326 Another major objective of this paper is to derive a robust calibration
 327 procedure of DISPATCH solely based on remotely sensed data.

328 In LINEAR mode, two different calibration strategies are tested on a
 329 daily and yearly time scale. In DAILY mode, a value of \mathbf{SM}_p is obtained
 330 for each SMOS pixel and daily input data set whereas in YEARLY mode, a
 331 single value of \mathbf{SM}_p is obtained for each SMOS pixel. The yearly calibration
 332 requires to run the daily calibration over the entire time series and average
 333 the daily \mathbf{SM}_p for each SMOS pixel.

334 In NONLINEAR mode, \mathbf{P} is computed daily from low-resolution \mathbf{SM} and
 335 \mathbf{SEE} , and \mathbf{SM}_p is set to the value estimated in YEARLY mode.

336 3.3. *New version of DISPATCH*

337 From the version described in Merlin et al. (2012b), the current version
 338 of DISPATCH differs in two main aspects: temperature endmembers are
 339 computed differently, and a correction for topographic effects is included.

340 3.3.1. *Temperature endmembers*

341 In the new version of DISPATCH, the minimum land surface temperature
 342 is selected among the pixels with the best land surface temperature quality
 343 index. For MODIS data, best quality is indicated by an index equal to
 344 0. Selecting only the best quality temperature data is an efficient way to
 345 remove atmospheric effects on the MODIS pixels partly contaminated by
 346 clouds/aerosols but still retained by the MODIS algorithm for the retrieval
 347 of land surface temperature.

348 In Merlin et al. (2012b), the estimation of maximum vegetation temper-
 349 ature was constrained using additional information provided by the MODIS-
 350 derived surface albedo (Merlin et al., 2010b). Herein, a simpler approach
 351 based on fractional vegetation cover only is adopted for two reasons: (i) sur-

face albedo is not an operational product from ASTER or Landsat data and
(ii) the approach in Merlin et al. (2010b, 2012b) was developed for brown
agricultural soils with relatively low albedo values and may not be valid in
other more heterogeneous soil conditions.

3.3.2. Topographic effects

To take into account the decrease of air temperature with altitude, a
simple correction is applied to land surface temperature data:

$$T_{corr} = T + \gamma(H - \mathbf{H}) \quad (13)$$

with T_{corr} being the topography-corrected land surface temperature, T the
land surface temperature derived from MODIS, ASTER or Landsat, γ ($^{\circ}\text{C}$
 m^{-1}) the mean lapse rate i.e. the negative of the rate of temperature change
with altitude change, H the altitude of the high-resolution optical pixel and
 \mathbf{H} the mean altitude within the low resolution pixel. Lapse rate is set to
 $0.006 \text{ } ^{\circ}\text{C m}^{-1}$. Although topographic effects are expected to be low over
the Urgell irrigation area, the correction in Equation (13) possibly makes
disaggregation more robust in the hilly surrounding area.

4. Application

The linearity of soil evaporative efficiency model and its calibration proce-
dure using SMOS/thermal data are tested by running DISPATCH in DAILY
and YEARLY modes, and in LINEAR and NONLINEAR modes. The daily
availability of MODIS data allows testing the DAILY and YEARLY modes at
3 km resolution. The high spatial resolution of ASTER/Landsat data allows

373 testing the LINEAR and NONLINEAR modes over the full soil moisture
374 range. In the latter case, the low-resolution data correspond to the aggre-
375 gated value within the 20 km square area of the 1 km resolution MODIS-
376 disaggregated SMOS soil moisture obtained in YEARLY mode. In each case,
377 DISPATCH results are compared with the in situ measurements aggregated
378 at corresponding resolution. Note that a one-day gap between SMOS over-
379 pass and ground sampling dates is allowed in the comparison because field
380 campaigns were made in one or two successive days.

381 *4.1. Evaluation strategies*

382 DISPATCH results are evaluated by two comparison strategies: the spatio-
383 temporal comparison over the entire time series (strategy 1), and the spatial
384 comparison at the daily time scale (strategy 2) between the remotely sensed
385 soil moisture products and the in situ measurements aggregated at corre-
386 sponding resolution.

387 According to strategy 1, the null-hypothesis is the temporal comparison
388 between SMOS soil moisture and the in situ measurements aggregated at the
389 SMOS resolution. The performance of DISPATCH is hence assessed by com-
390 paring over the entire time series the disaggregated soil moisture with the in
391 situ measurements aggregated at corresponding resolution: 3 km for MODIS-
392 disaggregated SMOS data and 100 m for both ASTER-disaggregated and
393 Landsat-disaggregated SMOS data. Such a comparison between the uncer-
394 tainty in SMOS data at 40 km resolution and the uncertainty in DISPATCH
395 data at 3 km and 100 m resolution provides a useful overall assessment of
396 the different soil moisture products.

397 According to strategy 2, the null-hypothesis is the UNIFORM mode of

DISPATCH defined by setting the second term of Equation (3) to zero, i.e. setting disaggregated soil moisture to SMOS soil moisture. The performance of DISPATCH is hence assessed by comparing at the daily time scale the disaggregated soil moisture with the in situ measurements aggregated at corresponding resolution: 3 km for MODIS-disaggregated SMOS data and 100 m for both ASTER-disaggregated and Landsat-disaggregated SMOS data. Such a comparison is useful to specifically evaluate the soil moisture spatial representation provided by DISPATCH at the sub-SMOS-pixel scale, by freeing from the spatio-temporal trends provided by SMOS data at 40 km resolution.

Table 2 presents the results of strategy 1 for the different application resolutions and modes of DISPATCH. At 40 km resolution, the temporal correlation between SMOS and aggregated in situ measurements is 0.59. At 3 km resolution, the spatio-temporal correlation between MODIS-disaggregated SMOS and aggregated in situ measurements is 0.67 (YEARLY mode). At 100 m resolution, the spatio-temporal correlation between ASTER-disaggregated SMOS and localized in situ measurements and between Landsat-disaggregated SMOS and localized in situ measurements is 0.73 and 0.86, respectively (LINEAR mode). Moreover, the mean difference and the root mean square difference between SMOS or disaggregated SMOS and the in situ measurements aggregated at corresponding resolution is systematically lower at 3 km and 100 m resolution than at 40 km resolution. DISPATCH thus improves the comparison between SMOS and in situ measurements. This is explained by i) the non-representativeness at the 40 km scale of the in situ measurements made in the very heterogeneous study area and ii) a relatively robust

423 representation of the soil moisture variability at the sub-SMOS-pixel scale.

424 Although strategy 1 is useful to characterize the overall spatio-temporal
425 performance of each soil moisture product, it has several disadvantages for
426 evaluating the soil moisture spatial representation at the sub-SMOS-pixel
427 scale. First, strategy 1 mixes the spatio-temporal trend provided by SMOS
428 data with the spatial trend provided by DISPATCH. Hence, separating the
429 gain in spatial representation associated with disaggregation is nontrivial.
430 Second, in the case where the error in disaggregation products is larger than
431 the error in SMOS data, strategy 1 does not allow the disaggregation per-
432 formance to be evaluated: disaggregation could either improve or degrade
433 the soil moisture spatial representation at the sub-SMOS-pixel scale. Third,
434 the statistics presented in Table 2 are not (strictly speaking) comparable.
435 For instance, the number of data points is 15 with SMOS data and 94 with
436 DISPATCH-Landsat data, and the range of soil moisture values is 0.02-0.18
437 m^3/m^3 at 40 km resolution and 0.02-0.48 m^3/m^3 at 100 m resolution.

438 Strategy 2 is better adapted to evaluate the soil moisture representation
439 at the sub-SMOS-pixel scale. It allows i) comparing DISPATCH results with
440 the null-hypothesis in the same conditions (same number of data points, and
441 same in situ soil moisture range), ii) undertaking this comparison at the sub-
442 SMOS-pixel scale so that the spatial trend provided by DISPATCH can be
443 easily separated from the spatial trend provided by SMOS data at 40 km
444 resolution and iii) undertaking this comparison at the daily time scale so
445 that the spatial trend provided by DISPATCH can be easily separated from
446 the temporal trend provided by SMOS data.

447 For the above reasons, hereafter the evaluation study of DISPATCH is

448 based on strategy 2 (Agam et al., 2007; Gao et al., 2012; Kim and Hogue,
449 2012; Merlin et al., 2010b, 2012b,a).

450 *4.2. Testing the calibration procedure at 3 km resolution*

451 Figures 5a, b and c plot the 3 km resolution SMOS soil moisture disaggre-
452 gated in UNIFORM, DAILY and YEARLY mode as a function of aggregated
453 in situ measurements. When comparing Figures 5a and 5b, one observes that
454 DISPATCH provides meaningful sub-pixel information. Especially, the slope
455 of the linear regression between disaggregated and in situ soil moisture is
456 systematically greater than zero and close to 1 in average (see Table 3).
457 However, data are significantly scattered around the 1:1 line. When compar-
458 ing Figures 5b and 5c, one observes that the YEARLY mode is more stable
459 than the DAILY mode. In particular, the scatter is much reduced and the
460 slope of the linear regression between disaggregated and in situ soil moisture
461 better stabilized at a value close to 1. Moreover, the standard deviation (rep-
462 resented by errorbars in Figure 5) of the downscaled soil moisture values with
463 an estimated uncertainty greater than $0.04 \text{ m}^3/\text{m}^3$ is reduced by about 50%
464 in the YEARLY mode. Hence, up to 50% of the uncertainty in downscaled
465 soil moisture may be associated to the uncertainty in daily retrieved $\mathbf{SM_p}$.
466 This interesting result indicates that i) retrieving $\mathbf{SM_p}$ from readily available
467 SMOS and MODIS data is a satisfying option, ii) setting $\mathbf{SM_p}$ to a constant
468 value improves disaggregation results, and iii) the linear approximation is
469 well adapted at kilometric resolution.

470 To assess the impact of fractional vegetation cover on DISPATCH results
471 in DAILY and YEARLY modes, Figure 5d, e and f plot the disaggregation
472 results obtained by selecting the 1 km resolution MODIS pixels with a frac-

473 tional vegetation cover lower than 0.5. Statistical results are presented
474 in Table 4. By selecting the MODIS pixels with $f_v < 0.5$, the correlation
475 coefficient between disaggregated and in situ soil moisture is increased from
476 0.6 to 0.7 and the slope of the linear regression is closer to 1. As expected,
477 the less vegetated the surface, the more accurate soil temperature retrieval
478 and disaggregated soil moisture. Generally speaking, optical-based disaggre-
479 gation methodologies of surface soil moisture should be implemented over
480 low-vegetated surfaces only, or by assuming that the surface soil moisture
481 below vegetation cover is representative of mean conditions.

482 Note that some values of disaggregated soil moisture are negative in Fig-
483 ures 5c and 5f. Negative values are possible in the disaggregation output
484 because i) DISPATCH distributes fine-scale values relatively to the mean
485 and ii) no constraint is applied to limit the range of disaggregated values.
486 The main advantage of keeping unphysical negative soil moisture values in
487 output is bringing to light inconsistent \mathbf{SM}_p values and/or a possible bias
488 in SMOS data. In this study, the presence of negative values down to -0.04
489 m^3/m^3 is consistent with a mean difference between disaggregated and in situ
490 soil moisture estimated as $-0.06 \text{ m}^3/\text{m}^3$. This result is also consistent with
491 recent and ongoing calibration/validation studies around the world, which
492 tend to indicate a general underestimation of SMOS data with respect to
493 0-5 cm soil moisture measurements (Al Bitar et al., 2012; dall’Amico et al.,
494 2012; Gherboudj et al., 2012; Sánchez et al., 2012). It is pointed out that no
495 Radio Frequency Interference (RFI) filtering was applied to SMOS data, in
496 order to maximize the spatio-temporal window of the comparison between
497 disaggregated SMOS and in situ data.

Figure 6 presents the images of SMOS soil moisture and the SMOS data disaggregated at 1 km resolution in YEARLY mode for SMOS overpass on DoY 229, (a rainfall occurred on DoY 243) DoY 244, DoY 245 and DoY 277. Figure 6 also presents the images at 1 km resolution of the standard deviation of the disaggregation output ensemble.

4.3. Testing the linear approximation at 100 m resolution

Figures 7a, b and c plot the 100 m resolution SMOS soil moisture disaggregated in UNIFORM, LINEAR and NONLINEAR mode using ASTER data as a function of in situ measurements for ground data on DoY 228-229 and DoY 277. When comparing Figures 7a and 7b, one observes that DISPATCH is able to provide some sub-pixel information, but the slope of the linear regression between disaggregated and in situ data is low in LINEAR mode. When comparing Figures 7b and 7c, one observes that the NONLINEAR mode significantly improves the slope and thus the spatial representation of 100 m resolution soil moisture. The statistical results reported in Table 5 indicate that the correlation coefficient between disaggregated and in situ data is approximately the same for LINEAR and NONLINEAR modes, while the slope of the linear regression is increased from about 0.2 to 0.5 when taking into account nonlinearity effects.

Figures 7d, e and f plot the 100 m resolution SMOS soil moisture disaggregated in UNIFORM, LINEAR and NONLINEAR mode using Landsat-7 data as a function of in situ measurements for ground data on DoY 228-229, DoY 244 and DoY 277. Table 6 reports statistical results in terms of correlation coefficient, slope of the linear regression, mean difference and root mean square difference between disaggregated and in situ data. The disaggregation

523 results using Landsat-7 data are compared with those obtained using ASTER
524 data. DISPATCH performances are remarkably consistent with both sensors.
525 Slightly better results are obtained with Landsat-7 than with ASTER data,
526 indicating that the simple derivation of land surface temperature using raw
527 Landsat-7 thermal radiances in Equation (1) and its underlying assumptions
528 (surface emissivity set to 1 and neglected atmospheric corrections) are ap-
529 propriate for the application of DISPATCH.

530 Figure 8 presents the images of the SMOS data disaggregated at 100
531 m resolution in NONLINEAR mode using Landsat-7 (DoY 228, DoY 244
532 and DoY 276) and ASTER (DoY 228 and DoY 276) data and for SMOS
533 overpasses on DoY 229, DoY 244, and DoY 277.

534 **5. Parameterizing evaporation efficiency at integrated spatial scales**

535 The disaggregation algorithm presented in this paper relies on the spa-
536 tial link between optical-derived soil evaporative efficiency and near-surface
537 soil moisture. If DISPATCH is able to provide reliable surface soil moisture
538 estimates at a range of spatial resolutions, then reciprocally, one may hy-
539 pothesize that the soil evaporative efficiency models used in Equation (4)
540 and Equation (6) are reliable representations at their application scale. It
541 is important to note however that DISPATCH also relies on the model used
542 to estimate soil evaporative efficiency from optical data, which currently de-
543 pends on soil temperature endmembers $\mathbf{T}_{s,\min}$ and $\mathbf{T}_{s,\max}$. In this paper,
544 the methodology for estimating temperature endmembers is solely based on
545 the high-resolution optical data within the low-resolution pixel, meaning that
546 the accuracy in $\mathbf{T}_{s,\min}$ and $\mathbf{T}_{s,\max}$ mostly relies on the representativeness of

547 the surface conditions met within the low-resolution pixel. For instance, the
548 maximum and minimum soil temperatures are expected to be biased in the
549 case of a uniformly wet and dry SMOS pixel, respectively. An interesting
550 point is that the representativeness of the surface conditions met within a
551 SMOS pixel would depend on the spatial resolution of optical data. In par-
552 ticular, the temperature range of land surface temperature is different for
553 MODIS and ASTER data (not shown) although they are associated with
554 the same surface conditions. Irrigated areas including both dry mature and
555 early stage wet crops (and possibly water reservoirs) do provide the het-
556 erogeneous conditions to estimate temperature endmembers accurately, as
557 long as the spatial resolution of the optical sensors is finer than the typical
558 field size. Consequently, the application of DISPATCH with 1 km resolution
559 MODIS data on one side and with 100 m resolution Landsat or ASTER data
560 on the other may require different soil evaporative efficiency representations
561 due to the lack of transferability across resolutions of the methodology used
562 for estimating temperature end-members.

563 The meaningfulness of the linear soil evaporative efficiency model in Equa-
564 tion (4) is investigated by plotting in Figure 9a the MODIS-derived soil evap-
565 orative efficiency aggregated at 40 km resolution as a function of SMOS soil
566 moisture for the entire time series from April to October 2011. While the
567 slope of the linear regression between aggregated MODIS-derived soil evapo-
568 rative efficiency and SMOS soil moisture is positive, no significant correlation
569 is observed. The non-uniqueness of the relationship between soil evaporative
570 efficiency and surface soil moisture in changing atmospheric conditions has
571 been reported in a number of studies (Chanzy and Bruckler, 1993; Merlin

et al., 2011). However, the SMOS-scale soil evaporative efficiency seems to be quasi constantly equal to 0.5, which is not consistent with the great soil moisture range covered by SMOS data. To further investigate the particular behaviour of aggregated MODIS-derived soil evaporative efficiency, the daily retrieved $\mathbf{SM_p}$ parameter is plotted in Figure 9b as a function of SMOS soil moisture. A strong correlation is visible with a slope of the linear regression between $\mathbf{SM_p}$ and SMOS soil moisture of about 2. Both results ($\mathbf{SEE} \sim 0.5$ and $\mathbf{SM_p}/\mathbf{SM} \sim 2$) tend to indicate that there is a significant compensation effect between \mathbf{SEE} and $\mathbf{SM_p}$ variations. It is thus highly probable that the daily variations in retrieved $\mathbf{SM_p}$ be partly due to the variations in \mathbf{SEE} associated with biased estimates of temperature endmembers $\mathbf{T_{s,min}}$ and $\mathbf{T_{s,max}}$.

The above discussion hypothesizes that a robust spatio-temporal estimation of temperature end-members $\mathbf{T_{s,min}}$ and $\mathbf{T_{s,max}}$ would help parameterizing soil evaporative efficiency at a range of spatial scales. Future studies may use a soil energy balance model to simulate the minimum and maximum soil temperatures with a better accuracy than using the methodology solely based on remote sensing optical data. This would require meteorological data composed of air temperature, solar radiation, wind speed and relative humidity at a 40 km resolution or finer. Note that in this case, DISPATCH would no longer operate with relative values since the algorithm would combine remotely sensed temperature with the temperature endmembers estimated from other ancillary data. Consequently, remotely sensed temperature data should be fully compatible with those simulated by the energy balance model. In particular, the simple approach used in the paper to estimate land surface

597 temperature from raw Landsat thermal radiances would no longer be valid
598 when using an energy balance model.

599 **6. Conclusion**

600 In this study, DISPATCH is applied to 40 km resolution SMOS soil mois-
601 ture data over an irrigated and dry land area in Catalunya, Spain. The
602 objective is to provide 1 km resolution surface soil moisture over a 60 km
603 60 km area from SMOS and 1 km resolution MODIS data and to provide
604 100 m resolution surface soil moisture over a 20 km by 20 km area from
605 MODIS-disaggregated SMOS and 100 m resolution Landsat and ASTER
606 data. Disaggregated soil moisture data are evaluated at 3 km resolution us-
607 ing in situ 0-5 cm measurements made once a month from April to October
608 2011, and at 100 m resolution using the ground data collected in August,
609 September and October.

610 To investigate the overall spatio-temporal performance of DISPATCH
611 soil moisture products, a first comparison is conducted over the entire time
612 series. At 40 km resolution, the temporal correlation between SMOS and
613 aggregated in situ measurements is 0.59. At 3 km resolution, the spatio-
614 temporal correlation between MODIS-disaggregated SMOS and aggregated
615 in situ measurements is 0.67. At 100 m resolution, the spatio-temporal cor-
616 relation between ASTER-disaggregated SMOS and localized in situ mea-
617 surements and between Landsat-disaggregated SMOS and localized in situ
618 measurements is 0.73 and 0.86, respectively. Moreover, the mean difference
619 and the root mean square difference between SMOS or disaggregated SMOS
620 and the in situ measurements aggregated at corresponding resolution is sys-

tematically lower at 3 km and 100 m resolution than at 40 km resolution. DISPATCH thus improves the comparison between SMOS and in situ measurements. This is explained by i) the non-representativeness at the 40 km scale of the in situ measurements made in the very heterogeneous study area and ii) a relatively robust representation of soil moisture variability at the sub-SMOS-pixel scale.

To specifically investigate the soil moisture spatial representation at the sub-SMOS-pixel scale, a second comparison is conducted at the daily time scale. At 3 km resolution, results indicate that (i) the mean daily correlation coefficient and the mean daily slope of the linear regression between disaggregated and in situ data is 0.7 and 0.8 respectively, (ii) a yearly calibration of the soil evaporative efficiency model makes the algorithm more robust with a greater stability of the slope around 1, and (iii) assuming a linear soil evaporative efficiency model is adequate at kilometric resolution. At 100 m resolution, results indicate with both Landsat and ASTER data a mean daily correlation coefficient between disaggregated SMOS and in situ data of about 0.7 but a low slope of the mean daily linear regression estimated as 0.2. When adding a correction for non-linearity effects between soil evaporative efficiency and surface soil moisture, the mean daily correlation coefficient between disaggregated SMOS and in situ data is kept relatively constant while the slope of the mean daily linear regression is improved from 0.2 to about 0.5.

If DISPATCH is able to provide reliable surface soil moisture estimates at a range of spatial resolutions, then reciprocally, one may hypothesize that the soil evaporative efficiency model used in the algorithm is a reliable represen-

646 tation at the application scale. However, compensation effects are identified
647 between optical-derived soil evaporative efficiency and the retrieved soil evap-
648 orative efficiency parameter. These compensation effects are attributed to
649 the methodology for estimating temperature endmembers solely based on re-
650 mote sensing data. DISPATCH could be a useful tool to help parameterize
651 soil evaporative efficiency at a range of spatial scales, but to do so, indepen-
652 dent meteorological data should be used to better constrain the temperature
653 endmembers in both space and time.

654 This study demonstrates the potential of DISPATCH for operational
655 multi-scale monitoring of surface soil moisture using readily available SMOS,
656 MODIS and Landsat/ASTER data. Due to the recent failure of Landsat-5,
657 the provision of high-resolution thermal data currently relies on on-request
658 ASTER and SLC-off Landsat-7 data. The Landsat Data Continuity Mis-
659 sion (LDCM), with increased coverage capabilities, is scheduled for launch
660 in 2013. In the medium term, the continuity of L-band derived soil moisture
661 data will be ensured by the SMAP mission, scheduled for launch in 2014.

662 **Acknowledgements**

663 Project RD10-1-0035 co-financed by the European Regional Development
664 Fund under the Catalan operational program 2007-2013.

665 **References**

- 666 Agam, N., Kustas, W. P., Anderson, M. C., Li, F., Neale, C. M. U., 2007.
667 A vegetation index based technique for spatial sharpening of thermal im-
668 agery. Remote Sens. Environ. 107, 545–558.

- 669 Al Bitar, A., Leroux, D., Kerr, Y. H., Merlin, O., Richaume, P., Sahoo,
670 A., Wood, E. F., 2012. Evaluation of SMOS soil moisture products over
671 continenal U.S. using the SCAN/SNOTEL network. IEEE Trans. Geosci.
672 Remote Sens. 50 (5), 1572–1586, doi:10.1109/TGRS.2012.2186581.
- 673 Budyko, M. I., 1956. Heat balance of the Earth’s surface. Gidrometeoizdat,
674 Leningrad.
- 675 Carlson, T., 2007. An overview of the ‘triangle method’ for estimating sur-
676 face evapotranspiration and soil moisture from satellite imagery. Sensors
677 7, 1612–1629.
- 678 Carlson, T. N., Gillies, R. R., Perry, E. M., 1994. A method to make use of
679 thermal infrared temperature and NDVI measurements to infer soil water
680 content and fractional vegetation cover. Remote Sens. Rev. 52, 45–59.
- 681 Chanzy, A., Bruckler, L., 1993. Significance of soil surface moisture with
682 respect to daily bare soil evaporation. Water Resour. Res. 29 (4), 1113–
683 1125.
- 684 Chauhan, N. S., Miller, S., Ardanuy, P., 2003. Spaceborne soil moisture es-
685 timation at high resolution: a microwave-optical/IR synergistic approach.
686 Int. J. Remote Sens. 24 (22), 4599–4622.
- 687 Cosby, B. J., Hornberger, G. M., Clapp, R. B., Ginn, T. R., 1984. A statis-
688 tical exploration of the relationships of soil moisture characteristics to the
689 physical properties of soils. Water Resour. Res. 20, 682–690.
- 690 dall’Amico, J. T., Schlenz, F., Loew, A., Mauser, W., 2012. First
691 results of SMOS soil moisture validation in the upper Danube

692 catchment. *IEEE Trans. Geosci. Remote Sens.* 50 (5), 1507–1516,
693 doi:10.1109/TGRS.2011.2171496.

694 Entekhabi, D., Njoku, E. G., O’Neill, P. E., Kellogg, K. H., Crow, W. T.,
695 Edelstein, W. N., Entin, J. K., Goodman, S. D., Jackson, T. J., Johnson,
696 J., Kimball, J., Piepmeier, J. R., Koster, R., Martin, N., McDonald, K. C.,
697 Moghaddam, M., Moran, S., Reichle, R., Shi, J. C., Spencer, M. W.,
698 Thurman, S. W., Tsang, L., Van Zyl, J., 2010. The Soil Moisture Active
699 Passive (SMAP) mission. *Proceedings of the IEEE* 98 (5), 704–716.

700 Gao, F., Kustas, W. P., Anderson, M. C., 2012. A data mining approach
701 for sharpening thermal satellite imagery over land. *Remote Sens.* 4, 3287–
702 3319, doi:10.3390/rs4113287.

703 Gherboudj, I., Magagi, R., Goita, K., Berg, A. A., Toth, B., Walker, A.,
704 2012. Validation of SMOS data over agricultural and boreal forest ar-
705 eas in Canada. *IEEE Trans. Geosci. Remote Sens.* 50 (5), 1623–1635,
706 doi:10.1109/TGRS.2012.2188532.

707 Hagolle, O., Huc, M., Pascual, D. V., Dedieu, G., 2010. A multi-temporal
708 method for cloud detection, applied to FORMOSAT-2, VENUS, LAND-
709 SAT and SENTINEL-2 images. *Remote Sens. Environ.* 114 (8), 1747–1755,
710 doi:10.1016/j.rse.2010.03.002.

711 Hemakumara, H. M., Kalma, J. D., Walker, J. P., Willgoose, G. R., 2004.
712 Downscaling of low resolution passive microwave soil moisture observa-
713 tions. In: *Proc. 2nd Int. CAHMDA Workshop Terrestrial Water Cycle*.
714 Princeton, NJ, pp. 67–73.

- 715 Hossain, A., Easson, G., Jul. 2008. Evaluating the potential of VI-LST tri-
716 angle model for quantitative estimation of soil moisture using optical im-
717 agery. In: Proc. IEEE Int. Geosci. Remote Sens. Symp. Boston, MA, pp.
718 III879–III882.
- 719 Jackson, T. J., Moran, M. S., O’Neill, P. E., 2008. Introduction to Soil Mois-
720 ture EXperiments 2004 (SMEX04). Remote Sens. of Environ. 112 (2), 301–
721 303.
- 722 Jiang, L., Islam, S., 2003. An intercomparison of regional latent heat flux
723 estimation using remote sensing data. Int. J. Remote Sens. 24, 2221–2236.
- 724 Kerr, Y. H., Waldteufel, P., Richaume, P., Ferrazzoli, P., Wigneron, J.-P.,
725 2011. SMOS level 2 processor soil moisture Algorithm Theoretical Ba-
726 sis Document (ATBD). Vol. SO-TN-ESL-SM-GS-0001, V3.4. CESBIO,
727 Toulouse, France.
- 728 Kerr, Y. H., Waldteufel, P., Richaume, P., Wigneron, J. P., Ferrazzoli, P.,
729 Mahmoodi, A., Al Bitar, A., Cabot, F., Gruhier, C., Leroux, D., Mialon,
730 A., Delwart, S., 2012. The SMOS soil moisture retrieval algorithm. IEEE
731 Trans. Geosci. Remote Sens. Doi:10.1109/TGRS.2012.2184548.
- 732 Kim, J., Hogue, T. S., 2012. Improving spatial soil moisture representa-
733 tion through integration of AMSR-E and MODIS products. IEEE Trans.
734 Geosci. Remote Sens. 50 (2), 446–460, doi:10.1109/TGRS.2011.2161318.
- 735 Komatsu, T. S., 2003. Towards a robust phenomenological expression of evap-
736 oration efficiency for unsaturated soil surfaces. J. Appl. Meteorol. 42, 1330–
737 1334.

- 738 Lee, T. J., Pielke, R. A., 1992. Estimating the soil surface specific humidity.
739 J. Appl. Meteor. 31, 480–484.
- 740 Manabe, S., 1969. Climate and the ocean circulation. I. The atmospheric
741 circulation and the hydrology of the Earth’s surface. Month. Weather Rev.
742 97 (11), 739–774.
- 743 Merlin, O., Al Bitar, A., Rivalland, V., Béziat, P., Ceschia, E., Dedieu, G.,
744 2011. An analytical model of evaporation efficiency for unsaturated soil
745 surfaces with an arbitrary thickness. J. Appl. Meteor. Clim. 50 (2), 457–
746 471, doi:10.1175/2010JAMC2418.1.
- 747 Merlin, O., Al Bitar, A., Walker, J. P., Kerr, Y., 2009. A sequential model
748 for disaggregating near-surface soil moisture observations using multi-
749 resolution thermal sensors. Remote Sens. Environ. 113 (10), 2275–2284,
750 doi:10.1016/j.rse.2009.06.012.
- 751 Merlin, O., Al Bitar, A., Walker, J. P., Kerr, Y., 2010a. An improved al-
752 gorithm for disaggregating microwave-derived soil moisture based on red,
753 near-infrared and thermal-infrared data. Remote Sens. Environ. 114 (10),
754 2305–2316, doi:10.1016/j.rse.2010.05.007.
- 755 Merlin, O., Duchemin, B., Hagolle, O., Jacob, F., Coudert, B., Chehbouni,
756 G., Dedieu, G., Garatuza, J., Kerr, Y., 2010b. Disaggregation of MODIS
757 Surface Temperature over an Agricultural Area Using a Time Series
758 of Formosat-2 Images. Remote Sens. Environ. 114 (11), 2500–2512,
759 doi:10.1016/j.rse.2010.05.025.

- 760 Merlin, O., Jacob, F., Wigneron, J.-P., Walker, J., Chehbouni, G.,
761 2012a. Multidimensional disaggregation of land surface temperature us-
762 ing high-resolution red, near-infrared, shortwave-infrared, and microwave-
763 L bands. *IEEE Trans. Geosci. Remote Sens.* 50 (5), 1864–1880,
764 doi:10.1109/TGRS.2011.2169802.
- 765 Merlin, O., Rüdiger, C., Al Bitar, A., Richaume, P., Walker, J. P.,
766 Kerr, Y. H., 2012b. Disaggregation of SMOS soil moisture in South-
767 eastern Australia. *IEEE Trans. Geosci. Remote Sens.* 50 (5), 1557–1571,
768 doi:10.1109/TGRS.2011.2175000.
- 769 Merlin, O., Rüdiger, C., Richaume, P., Al Bitar, A., Mialon, A., Walker, J. P.,
770 Kerr, Y., 2010c. Disaggregation as a top-down approach for evaluating 40
771 km resolution SMOS data using point-scale measurements: application
772 to AACES-1. In: *SPIE, Remote Sensing of Agriculture, Ecosystems, and*
773 *Hydrology XII*. Toulouse, France, pp. 78240I–1–8, doi:10.1117/12.865751.
- 774 Merlin, O., Walker, J. P., Chehbouni, A., Kerr, Y., 2008. Towards
775 deterministic downscaling of SMOS soil moisture using MODIS de-
776 rived soil evaporative efficiency. *Remote Sens. Environ.* 112, 3935–3946,
777 doi:10.1016/j.rse.2008.06.012.
- 778 Moran, M. S., Clarke, T. R., Inoue, Y., Vidal, A., 1994. Estimating crop wa-
779 ter deficit using the relation between surface-air temperature and spectral
780 vegetation index. *Remote Sens. Environ.* 49, 246–263.
- 781 Njoku, E., Jackson, T., Lakshmi, V., Chan, T., Nghiem, S., 2003. Soil mois-

782 ture retrieval from AMSR-E. *IEEE Trans. Geosci. Remote Sens.* 41, 215–
783 229.

784 Noilhan, J., Planton, S., 1989. A simple parameterization of land surface
785 processes for meteorological models. *Mon. Wea. Rev.* 117, 536–549.

786 Peischl, S., Walker, J. P., Ye, C. R. N., Kerr, Y. H., Kim, E., Bandara, R.,
787 Allahmoradi, M., 2012. The AACES field experiments: SMOS calibration
788 and validation across the Murrumbidgee river catchment. *Hydrol. Earth*
789 *Sci. Discuss.* 9, 2763–2795, doi:10.5194/hessd-9-2763-2012.

790 Petropoulos, G., Carlson, T., Wooster, M., Islam, S., 2009. A review of Ts/VI
791 remote sensing based methods for the retrieval of land surface energy fluxes
792 and soil surface moisture. *Prog. Phys. Geography* 33 (2), 224–250.

793 Piles, M., Camps, A., Vall-llossera, M., Corbella, I., Panciera, R., Rüdiger,
794 C., Kerr, Y. H., Walker, J. P., 2011. Downscaling SMOS-derived soil mois-
795 ture using MODIS visible/infrared data. *IEEE Trans. Geosci. and Remote*
796 *Sens.* 49 (9), 3156–3166, doi:10.1109/TGRS.2011.2120615.

797 Sánchez, N., Martínez-Fernández, J., Pérez-Gutiérrez, C., 2012. Valida-
798 tion of the SMOS L2 soil moisture data in the REMEDHUS net-
799 work (Spain). *IEEE Trans. Geosci. Remote Sens.* 50 (5), 1602–1611,
800 doi:10.1109/TGRS.2012.2186971.

801 Saxton, K. E., Rawls, W. J., Romberger, J. S., Papendick, R. I., 1986. Esti-
802 mating Generalized Soil-water Characteristics from Texture. *Soil Sci. Soc.*
803 *Amer. J.* 50 (4), 1031–1036.

804 Zhan, X., Miller, S., Chauhan, N., Di, L., Ardanuy, P., 2002. Soil mois-
805 ture visible/infrared radiometer suite algorithm theoretical basis docu-
806 ment. Vol. Tech. Rep. Raytheon Syst. Company, Lanham, MD.

Table 1: Mean and standard deviation (std) of 0-5 cm deep in situ soil moisture measurements. Results are presented for each field campaign, and over the dryland and irrigated area separately.

Month	Dryland area	Irrigated area
	Mean (std)	Mean (std)
	m ³ /m ³	m ³ /m ³
Apr	0.012 (0.002)	0.017 (0.003)
May	0.075 (0.025)	0.10 (0.078)
Jun	0.12 (0.051)	0.19 (0.073)
Jul	0.081 (0.029)	0.15 (0.085)
Aug	0.021 (0.006)	0.16 (0.072)
Sep	- (-)	0.23 (0.047)
Oct	0.032 (0.017)	0.066 (0.027)

Table 2: Correlation coefficient (R), slope of the linear regression, mean difference (bias) and root mean square difference (RMSD) between SMOS or DISPATCH SM and the in situ measurements aggregated at corresponding resolution: 40 km for SMOS SM, 3 km for MODIS-disaggregated SMOS SM, and 100 m resolution for ASTER- and Landsat-disaggregated SMOS SM. The number of data points and the minimum and maximum values of aggregated in situ measurements are also reported.

Data	Spatial resolution	Thermal data	DISPATCH mode	R (-)	Slope (-)	Bias (m^3/m^3)	RMSD (m^3/m^3)	Number of data points	In situ SM range (m^3/m^3)
SMOS	40 km	none	none	0.59	0.25	-0.099	0.12	15	0.02-0.18
DISPATCH	3 km	MODIS	DAILY	0.58	0.46	-0.077	0.11	54	0.02-0.32
DISPATCH	3 km	MODIS	YEARLY	0.67	0.40	-0.084	0.11	54	0.02-0.32
DISPATCH	100 m	ASTER	LINEAR	0.73	0.18	-0.049	0.090	79	0.02-0.48
DISPATCH	100 m	Landsat	LINEAR	0.86	0.32	-0.068	0.11	94	0.02-0.48
DISPATCH	100 m	ASTER	NONLINEAR	0.69	0.50	-0.031	0.073	79	0.02-0.48
DISPATCH	100 m	Landsat	NONLINEAR	0.83	0.48	-0.052	0.090	94	0.02-0.48

Table 3: Mean (and standard deviation of) daily correlation coefficient (R), slope of the linear regression, mean difference (bias) and root mean square difference (RMSD) between disaggregated SMOS SM and in situ measurements aggregated at 3 km resolution. Comparison results are presented for all the 1 km MODIS pixels.

Mode	R (-)	Slope (-)	Bias (m ³ /m ³)	RMSD (m ³ /m ³)
UNIFORM	0.34 (0.55)	0.01 (0.02)	-0.11 (0.038)	0.12 (0.039)
DAILY	0.61 (0.33)	0.73 (0.96)	-0.071 (0.059)	0.093 (0.046)
YEARLY	0.61 (0.32)	0.58 (0.45)	-0.079 (0.055)	0.092 (0.047)

Table 4: Mean (and standard deviation of) daily correlation coefficient (R), slope of the linear regression, mean difference (bias) and root mean square difference (RMSD) between disaggregated SMOS SM and in situ measurements aggregated at 3 km resolution. Comparison results are presented for the 1 km MODIS pixels with a fractional vegetation cover lower than 0.5.

Mode	R (-)	Slope (-)	Bias (m ³ /m ³)	RMSD (m ³ /m ³)
UNIFORM	-0.07 (0.60)	0.01 (0.03)	-0.081 (0.057)	0.093 (0.051)
DAILY	0.70 (0.32)	0.86 (0.70)	-0.057 (0.052)	0.078 (0.036)
YEARLY	0.71 (0.32)	0.78 (0.31)	-0.067 (0.050)	0.079 (0.038)

Table 5: Daily correlation coefficient (R), slope of the linear regression, mean difference (bias) and root mean square difference (RMSD) between the SMOS SM disaggregated at 100 m resolution using ASTER data and localized in situ measurements. Comparison results are presented for each SMOS overpass date separately: DoY 229, DoY 244, DoY 277.

Mode	R (-)	Slope (-)	Bias (m ³ /m ³)	RMSD (m ³ /m ³)
UNIFORM	0.00, -, 0.00	0.00, -, 0.00	-0.071, -, -0.029	0.14, -, 0.047
LINEAR	0.80, -, 0.42	0.18, -, 0.20	-0.070, -, -0.029	0.12, -, 0.045
NONLINEAR	0.77, -, 0.37	0.51, -, 0.48	-0.045, -, -0.017	0.089, -, 0.053

Table 6: Daily correlation coefficient (R), slope of the linear regression, mean difference (bias) and root mean square difference (RMSD) between the SMOS SM disaggregated at 100 m resolution using Landsat-7 data and localized in situ measurements. Comparison results are presented for each SMOS overpass date separately: DoY 229, DoY 244, DoY 277.

Mode	R (-)	Slope (-)	Bias (m ³ /m ³)	RMSD (m ³ /m ³)
UNIFORM	0.00, 0.00, 0.00	0.00, 0.00, 0.00	-0.069, -0.18, -0.029	0.14, 0.19, 0.047
LINEAR	0.81, 0.40, 0.60	0.16, 0.073, 0.28	-0.068, -0.17, -0.028	0.12, 0.17, 0.041
NONLINEAR	0.80, 0.40, 0.55	0.43, 0.26, 0.65	-0.054, -0.14, -0.017	0.095, 0.15, 0.043

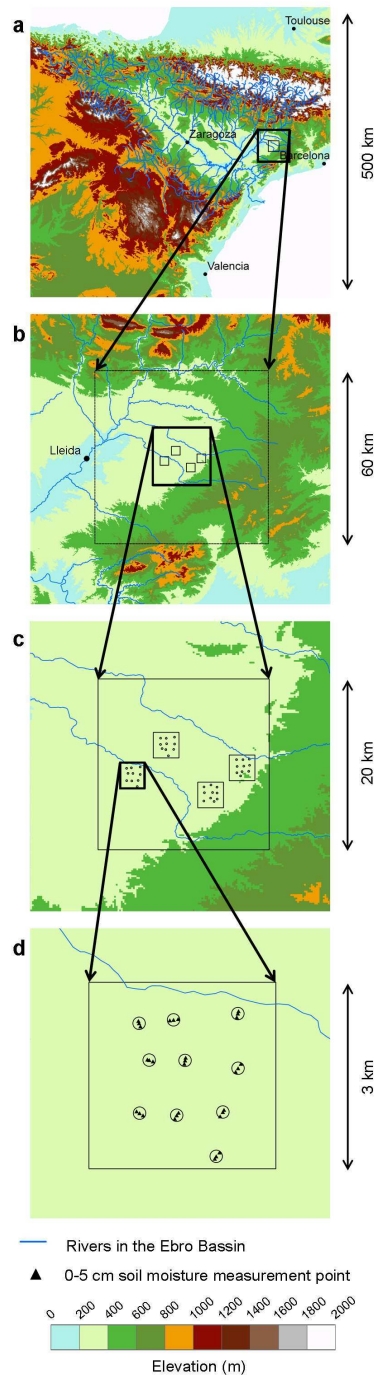


Figure 1: Overview of the study area and the ground sampling strategy.

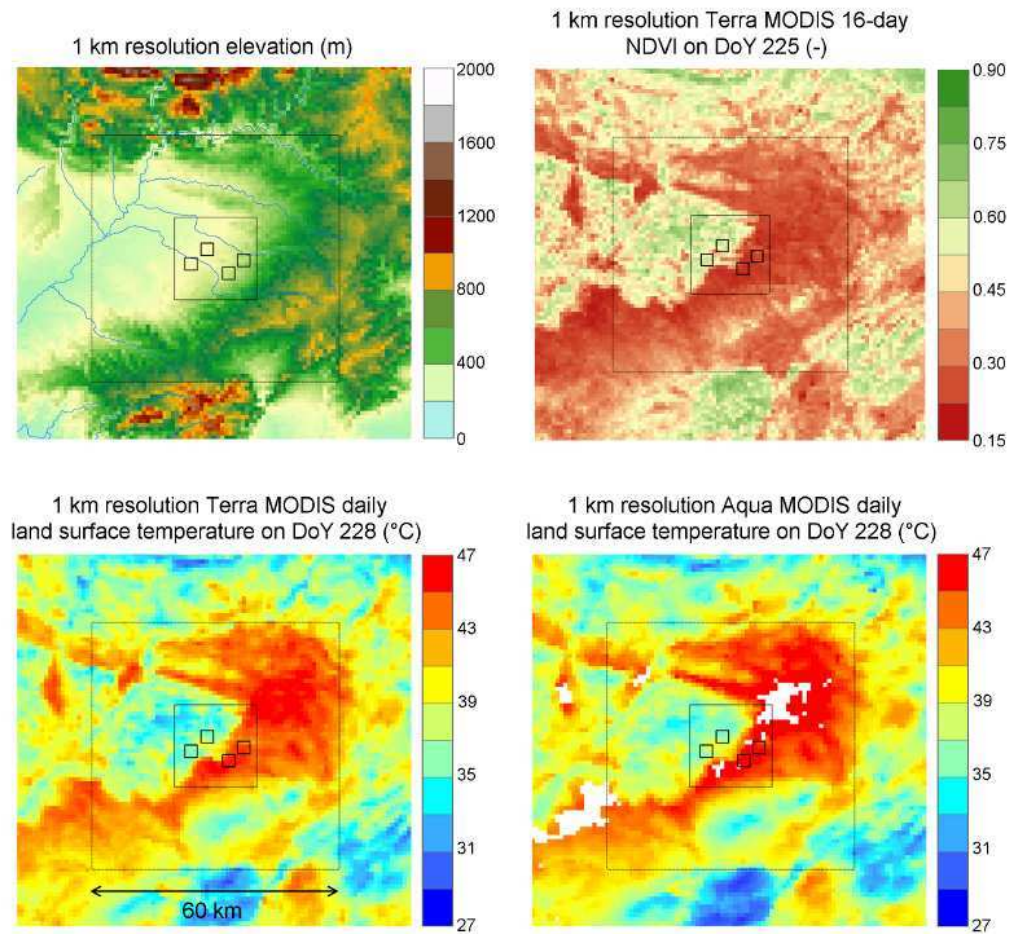


Figure 2: Images at 1 km resolution of elevation, Terra MODIS NDVI on Doy 225, Terra MODIS land surface temperature on DoY 228 (10:30 am) and Aqua MODIS land surface temperature on DoY 228 (1:30 pm).

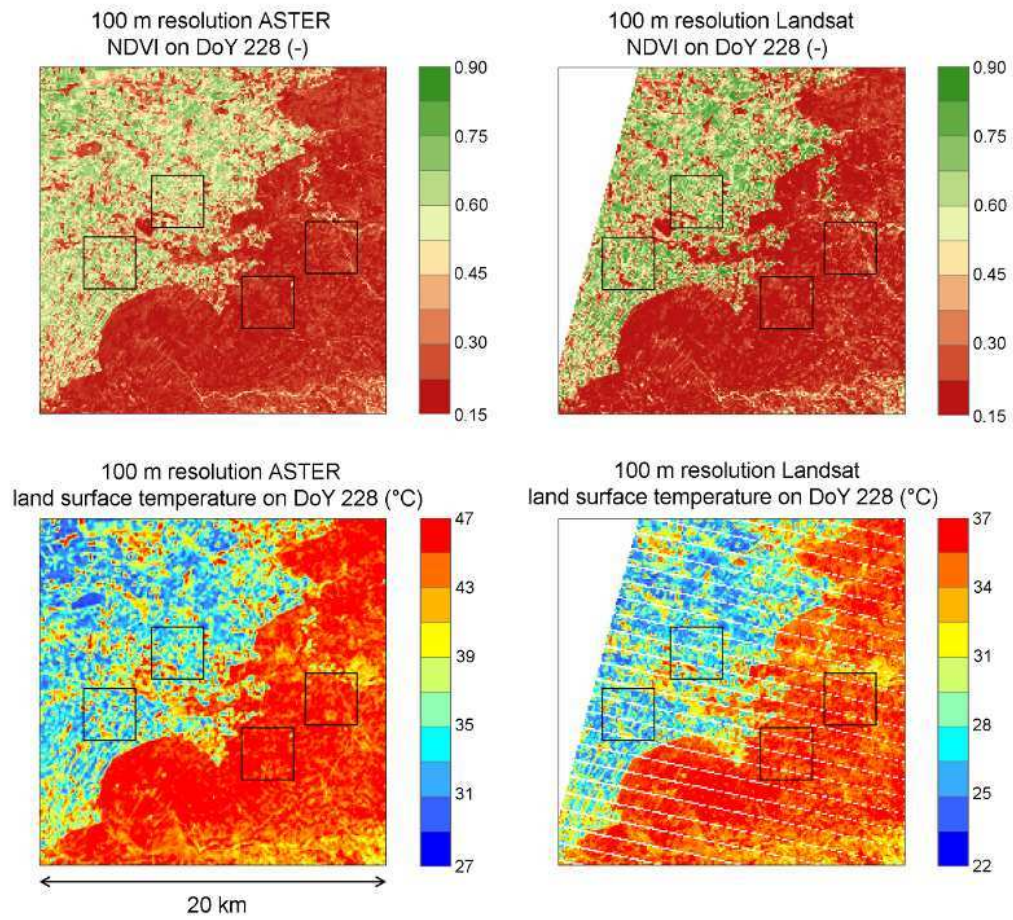


Figure 3: Images at 100 m resolution over the 20 km square area of ASTER- and Landsat-derived NDVI, and land surface temperature on DoY 228.

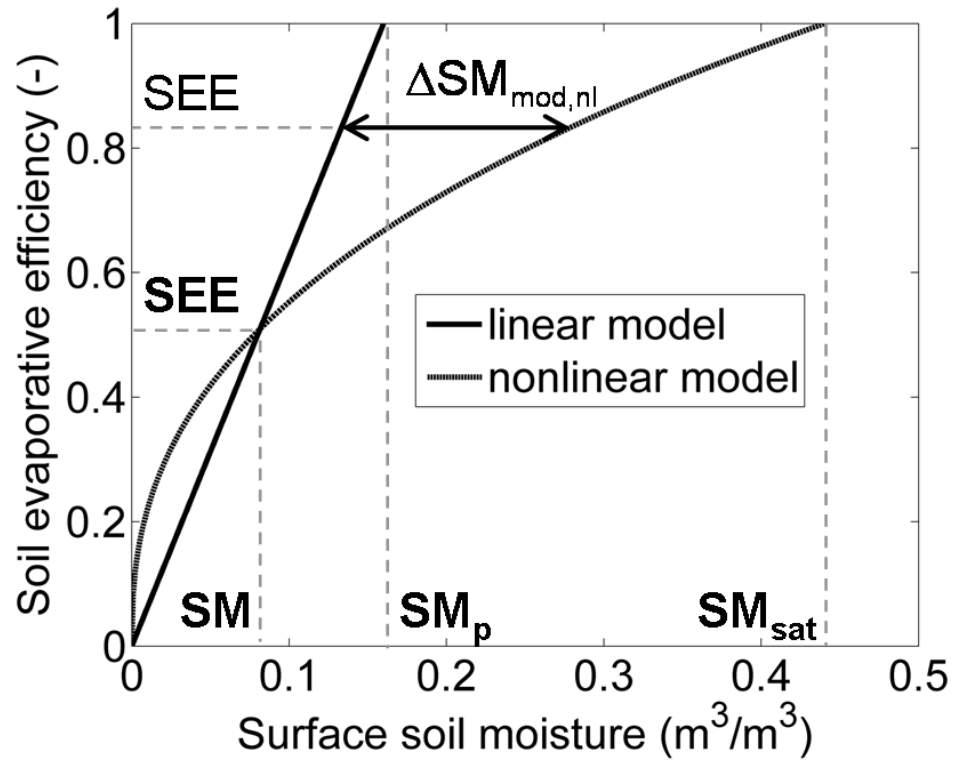


Figure 4: Soil evaporative efficiency modelled by the linear and nonlinear model versus surface soil moisture. The difference between inverse models is used to correct disaggregation output for nonlinearity effects.

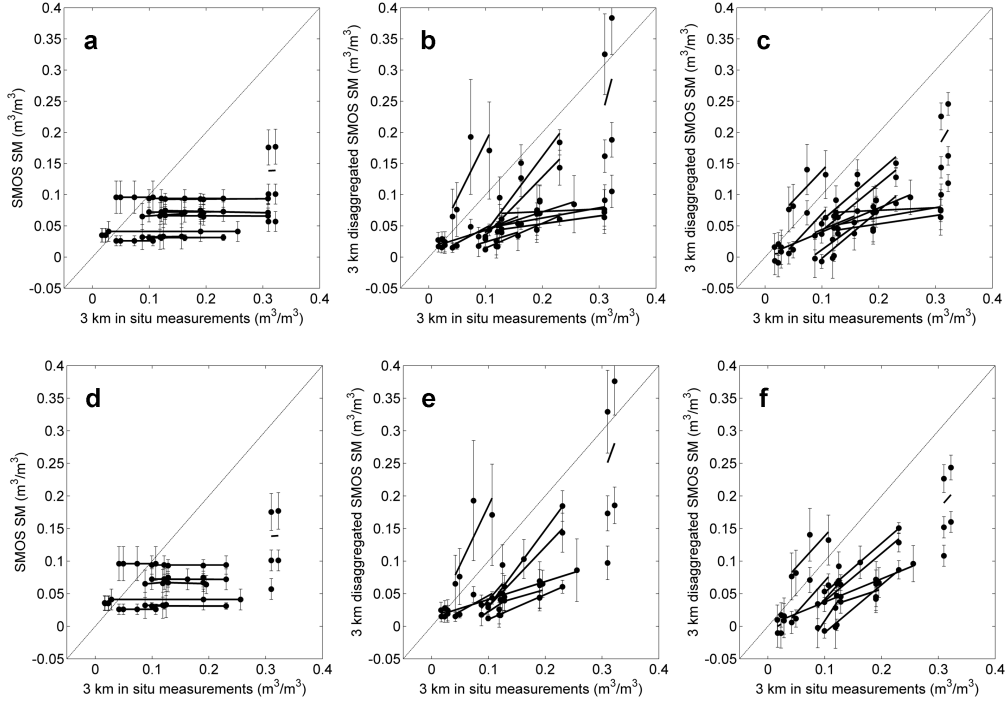


Figure 5: The SMOS soil moisture disaggregated in the UNIFORM (a and d), DAILY (b and e) and YEARLY (c and f) mode is plotted as a function of in situ measurements aggregated at 3 km resolution for all the MODIS pixels (top), and for the MODIS pixels with $f_v < 0.5$ (bottom). Errorbars represent the standard deviation of disaggregation output ensemble for each 3 km by 3 km ground sampling area, and the segments are the linear fit of daily data.

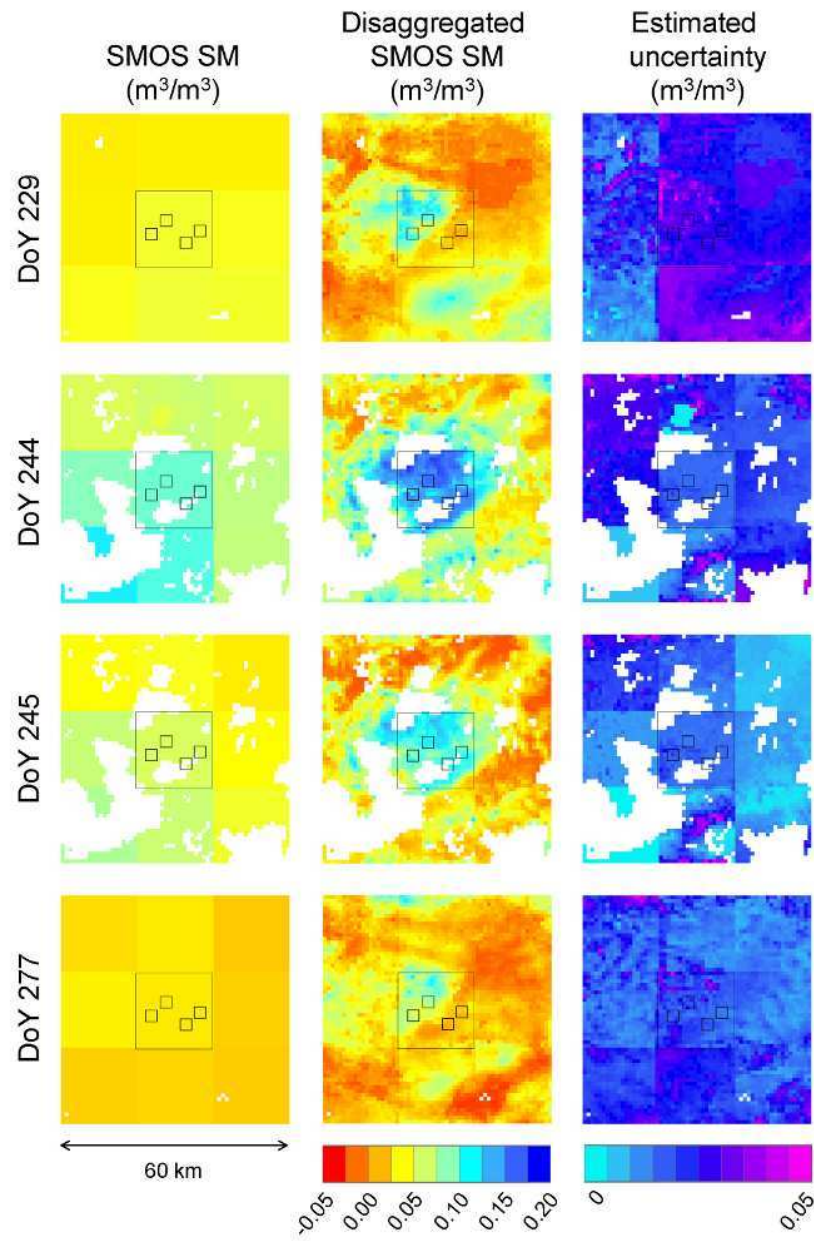


Figure 6: Images of SMOS soil moisture, the SMOS data disaggregated at 1 km resolution in YEARLY mode, and the estimated uncertainty in disaggregated data for SMOS overpass on DoY 229, DoY 244, DoY 245 and DoY 277.

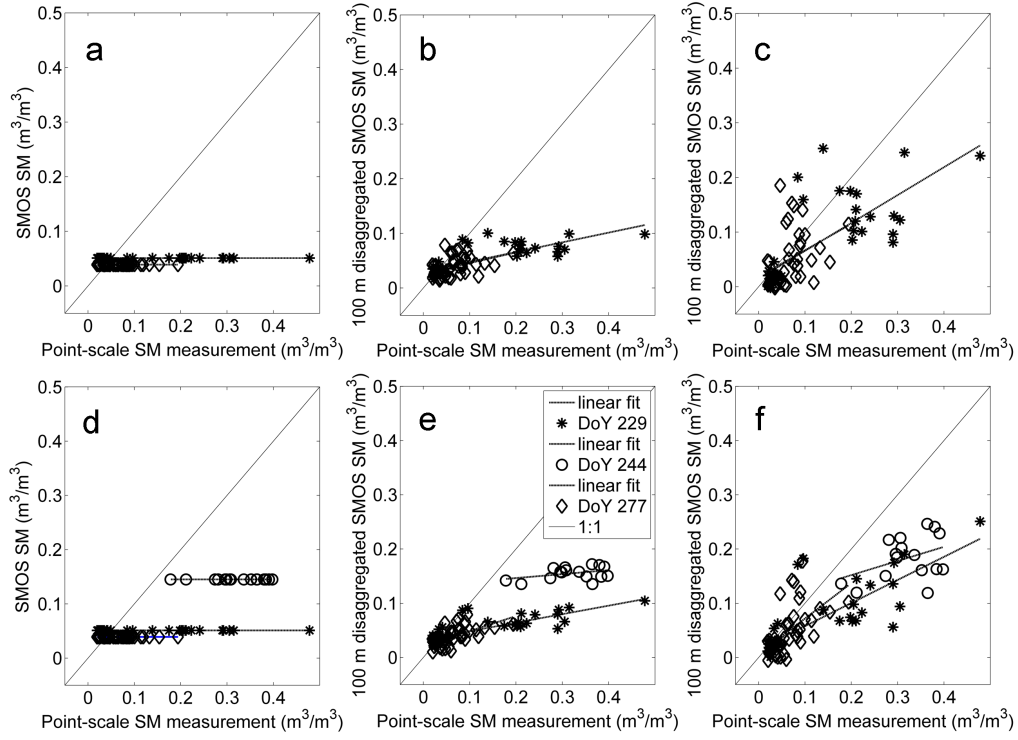


Figure 7: The SMOS soil moisture disaggregated at 100 m resolution in the UNIFORM (a and d), LINEAR (b and e) and NONLINEAR (c and f) mode is plotted as a function of localized situ measurements for ASTER data (top), and Landsat-7 data (bottom). The segments represent the linear fit of daily data.

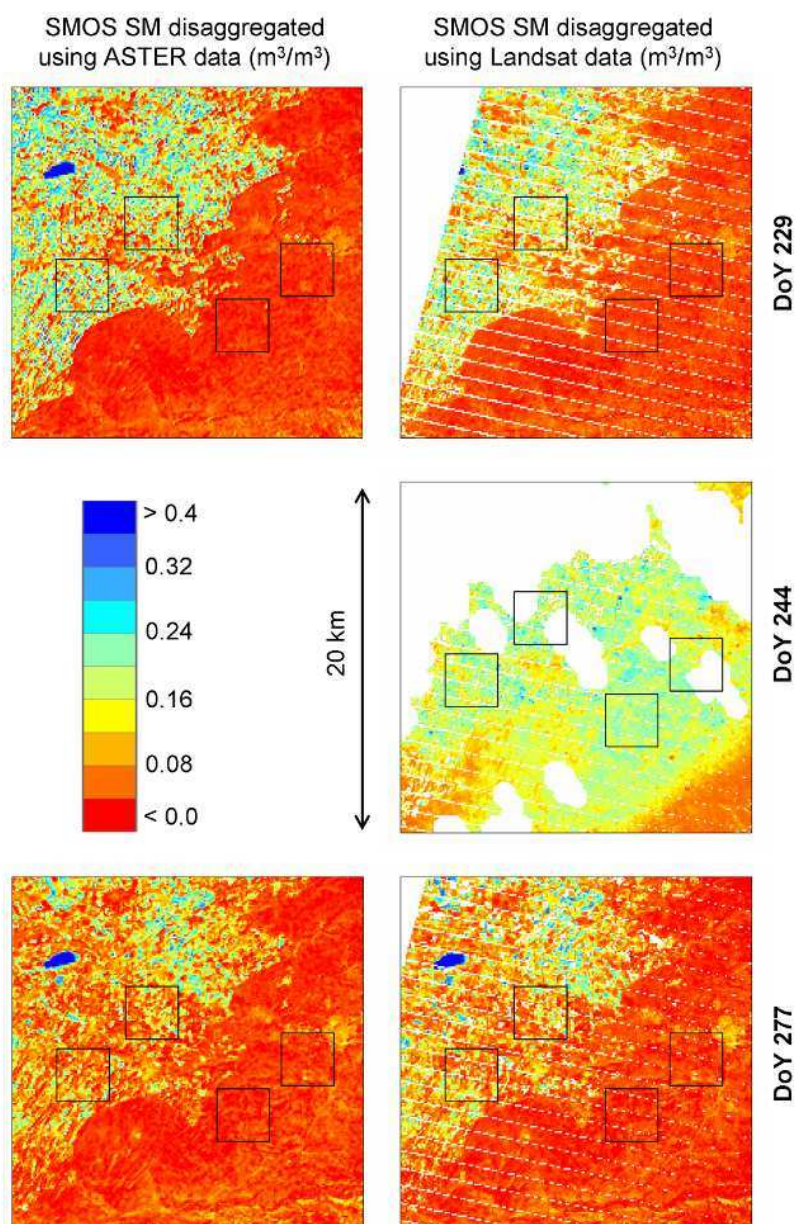


Figure 8: Images of the SMOS data disaggregated at 100 m resolution in NONLINEAR mode using ASTER (left) and Landsat-7 (right) data.

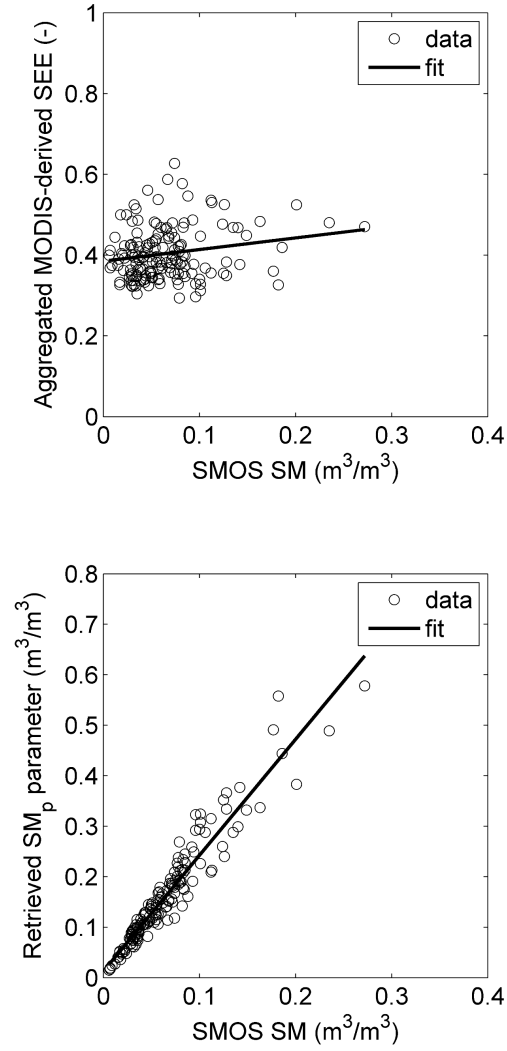


Figure 9: The MODIS-derived SEE aggregated at 40 km resolution (top), and the daily SM_p parameter retrieved over the study area (bottom) is plotted as a function of SMOS soil moisture for the entire time series spanning from April to October 2011.